ORIGINAL RESEARCH

Terminalia Catappa Fallen Leaves Stabilized Zirconia Nanoparticles for Enhanced Anticancer and Antibacterial Activities

Article History
Received: 01-Jun-2025
Revised: 21-Jun-2025
Accepted: 20-Jul-2025
Published: 02-Aug-2025

Raman Suresh[a*], Periyasamy Settu[b], Pitchaipillai Baskaran[c], Natarajan Thangamani[d], Paramasivam Sumathi[e], Ramasamy Subramanian[f*]

Abstract: Zirconia nanoparticles (ZrO_2 NPs) are eco-friendly and biocompatible materials used for various biological applications. Herein, we reported *Terminalia catappa* (*T. catappa*) fallen leaves extract encapsulated ZrO_2 NPs without using a chemical reducing agent. The bandgap, absorption, functional groups, and crystalline structure were identified using a UV-Visible spectrophotometer (UV-Vis), a Fourier transform infrared spectrometer (FT-IR), and an X-ray diffractometer. The transmission electron microscope (TEM) images confirmed the formation of spherical particles with an average size of 6 nm. The absorption in the range of 299–307 nm confirmed the formation of ZrO_2 NPs. The stretching vibration bands at 467 and 621 cm^{-1} confirmed the presence of the Zr–O–Zr bond in ZrO_2 NPs. According to the X-ray diffraction pattern (XRD), the average crystallite size of the ZrO_2 NPs was 4 nm with a cubic structure. The nanoparticles Zr0.01, Zr0.02, and Zr0.03 exhibited 26-, 28-, and 32-mm zones of inhibition against *Lactobacillus acidophilus, Staphylococcus albus*, and *Streptococcus mutans* at a maximum concentration of 25 µg/ml. The ZrO_2 exhibited an IC_{50} value of ZrO_2 to be 32.63 µg/mL against A549 cell lines. Therefore, biogenic *T. catappa* extract-encapsulated zirconia nanoparticles can be used for the development of potential antibacterial and anticancer agents.

Keywords: Zirconia nanoparticles, *Terminalaia catappa*, Oral bacteria, Cell viability, Anticancer activity

a Department of Chemistry, Government Polytechnic College, Tiruvannamalai 606705, Tamil Nadu, India.
b Department of Physics, Government Polytechnic College, Sankarapuram, Kallakurichi 606404 Tamil Nadu, India.
c Department of Physics, Government Arts and Science College, Veppanthattai, Perambalur, Tamil Nadu, India.
d Department of Chemistry, Trinity College for Women, Namakkal 637002, Tamil Nadu, India.
e Department of Chemistry, Gobi Arts & Science College (Autonomous), Gopichettipalayam 638476, Erode, Tamil Nadu, India
f Hydrolina Biotech Pvt Ltd, SIPCOT, Pochamballi, Krishnagiri, Tamil Nadu 635304, India.
* **Corresponding Author's Email:** rsureshivan2@gmail.com and ksrcassubu@gmail.com (Both authors have equal contribution)

1. INTRODUCTION

Nanotechnology has numerous applications in the field of materials science and technology. Nanotechnology deals with metal and metal oxide nanoparticles and their applications (De Jesus *et al.*, 2024). These nanomaterials have drawn the attention of researchers due to their properties and utility (Altammar, 2023). Chemical synthesis has various disadvantages, including environmental pollution, being hazardous to humans, long time consumption, and costly chemicals (Banjara *et al.*, 2024). Among the metal oxides, zirconia nanoparticles are among the most important due to their applications. ZrO_2 NPs are of immense interest due to their enhanced optical, dielectric, and piezoelectric properties. Zirconia is also promising as a significant type of catalyst (Nisha *et al.*, 2022; Wang *et al.*, 2021; Castellin *et al.*, 2021). Over the last two decades, few researchers have focused on the green synthesis of ZrO_2 NPs for various applications. Tropical almond is an underutilized fruit that is rich in antioxidants, vitamins, and pigments (Weerasekara *et al.*, 2015). Its fruits are eaten especially by humans, birds, and animals (Dos Santos *et al.*, 2016). *Terminalia catappa* is one of the trees containing numerous phenolic compounds, which have

many medicinal properties (Suresh Ramanan *et al*., 2025). *T. catappa* Linn is a tropical tree belonging to Southeast Asia, and it contains gallic acid, corilagin, ellagic acid, rutin, kaempferol, chebulagic acid, punicalagin, punicalin, and quercetin (Monks *et al*., 1991; Suriyaraj *et al*., 2019).

T. catappa L. leaves contain phenolic compounds such as gallic acid, kaempferol, and Kaempferol 3, 7, 4′-trimethyl ether (Ho *et al*., 2022). *T. catappa* L. leaves have radical scavenging activity, anti-inflammatory, antidepressant, antifungal, and chemopreventive activities (Wangui *et al*., 2024). Based on the medicinal properties, *T. catapa* fallen red leaves are rich in phenolic compounds, which are freely soluble in water. Few researchers have used *T. catappa* extract to produce various nanoparticles for various applications, as presented in **Table 1**.

Table 1. Synthesis of metal and metal oxide nanoparticles.

S. No.	Plant parts	Nanoparticles	References
1	*Terminalia catappa* leaf extract	Silver nanoparticles	Lipsa *et al*., 2023
2	*Terminalia catappa* leaf extract	Silver nanoparticles	Aishwarya *et al*., 2017
3	*Terminalia catappa* Leaf Extract	ZnO nanoparticles	Razieh *et al*., 2022
4	*Terminalia catappa* Leaf Extract	Silver nanoparticles	Muthulakshmi *et al*., 2022
5	*Terminalia catappa* Leaf Extract	Gold nanoparticles	Balaprasad, 2010
6	*Terminalia catappa* leaf extract	Cu_2O nanoparticles	Thi Hoai *et al*., 2024
7	*Terminalia catappa* leaf extract	Nickel ferrite nanoparticles	Sarala *et al*., 2022
8	*Terminalia catappa* leaf extract	ZnO nanoparticles	Momoh *et al*., 2024
9	*Cinnamon* extract	ZrO_2 Nanoparticles	Veerabhadraswamy *et al*., 2024
10	*Punica granatum* peel extract	ZrO_2 Nanoparticles	Tan *et al*., 2022
11	Ginger and garlic extract	ZrO_2 Nanoparticles	Chowdhury *et al*., 2023
12	*Parkia biglandulosa* leaf extract	ZrO_2 Nanoparticles	Muthulakshmi *et al*., 2023
13	*Sphagneticola trilobata* Leaf	ZrO_2 Nanoparticles	Kazi *et al*., 2022
14	*Sapindus mukorossi* pericarp extract	ZrO_2 Nanoparticles	Annu *et al*., 2022

Among the researchers, Muthulakshmi *et al*., (2023) have listed most of the plant extracts used in the green synthesis of zirconia nanoparticles. However, the extraction of the phenolic-rich part from the fruit of *T. catappa* as a reducing agent for ZrO_2 nanoparticles has yet to be studied. In this work, *T. catappa* fruit extract is considered a natural reducing agent to synthesize ZrO_2 nanoparticles for the anticancer activity.

2. MATERIALS AND METHODS

2.1. Reagent

Zirconium oxychloride, ethanol, and acetone were purchased from LobaChemie Pvt. Ltd., Mumbai, India. Zirconium oxychloride solution was prepared using distilled water. All the reagents (AR grade) used in this work were received as such without further purification.

2.2. Preparation of *T. catappa* extract

Fallen red leaves of *T. catappa* were collected from the Polytechnic College Campus, Nagapadi, Tamil Nadu, India. The leaves were thoroughly washed with running tap water, cut into small pieces, and boiled for 30 minutes at 85ºC in 200 mL of distilled water. The extract was filtered through muslin cloth, followed by Whatman 1 filter paper, and stored in the refrigerator. Three different concentrations of zirconium salt (0.01, 0.02, and 0.03 M) solutions were prepared using distilled water.

2.3. Synthesis of ZrO_2 NPs

Three different concentrations of zirconium precursor salt solution, Zr0.01, Zr0.02, and Zr0.03 and extract volumes of 10, 20, and 30 mL were used, respectively, to investigate the effect of precursor and extract concentrations on the synthesis process. In the typical procedure, zirconium salt solution (0.01,

0.02, and 0.03 M), 100 mL, was placed in a 250 mL beaker, stirred with a magnetic stirrer, and heated at 85°C. The extracts, 10, 20, and 30 mL, were dropwise added to 0.01, 0.02, and 0.03 M zirconium salt solutions, and continued mixing with heating resulted in an off-white precipitate. The precipitate was carefully collected and washed with distilled water. It was dried in a hot air oven at 85°C and annealed at 500°C for 3 hours to get ZrO_2 NPs. The ZrO_2 NPs synthesised from 0.01, 0.02, and 0.03 M zirconium salt solution were named Zr0.01, Zr0.02, and Zr0.03, respectively.

2.4. Materials Characterization

The absorption maximum of the samples was recorded using a UV-Visible spectrophotometer (HR-2UVV250-10 Spectrometer). An FT-IR spectrometer was used to carry out functional group identification (Perkin Elmer, Spectrum 2). X-ray diffractometers (Rigaku, Miniflex) analyzed the samples' crystalline phase. The formation of particles was analyzed by scanning electron microscopy with energy dispersive X-ray analysis (TESCAN OXFORD, SEM with EDAX). The morphology of the samples was examined by transmission electron microscopy (FEI Tecnai G220 S-TWIN HR-TEM) coupled with a selected area diffraction pattern (SAED).

2.5. Antibacterial Activity

Clinical isolates of *Lactobacillus acidophilus*, *Staphylococcus albus*, and *Streptococcus mutans* were obtained from Coimbatore Medical College Hospital, Tamil Nadu. The bacterial cultures were maintained in the nutrient broth at 37°C. These bacteria were developed in 5 mL of sterile nutrient broth at 37ºC for 24 hours. To access the minimum inhibitory concentration (MIC), a set of Mueller-Hinton broth in 5 tubes was prepared under sterile conditions for each test organism. About 100 µL of an appropriate concentration of ZrO_2 NPs was added to test tubes containing Mueller-Hinton broth. After that, 10 µL of test culture suspension was added to the broth and incubated at 37ºC for 24 hours. The MIC was determined using the lowest dilution inhibiting the growth of bacteria. The zone of inhibition was expressed in millimeters (Muthulakshmi *et al*., 2023). The diameter of the zone of inhibition was expressed in mm. Amoxicillin (10 µg) was the reference material, and DMSO solvent was the control.

2.6. Anticancer Activity

The human lung cancer cell line (A549) was provided by the National Centre for Cell Science (NCCS) in Pune, India, and was cultured in Eagle's Minimum Essential Medium with 10% foetal bovine serum (FBS) at 37°C, 5% CO_2, 95% air, and 100% relative humidity to maintain the cells. Weekly passages of maintenance cultures and biweekly medium changes were performed. Trypsin-ethylene diamine tetraacetic acid (EDTA) was used to separate the monolayer cells into single-cell suspensions, and viable cells were counted using a hemocytometer. The single-cell suspensions were then diluted with media containing 5% FBS to give a final density of 1×10^5 cells/mL. Totally 10,000 cells were seeded onto 96-well plates using 100 µL of cell suspension per well, and the plates were then incubated at 37°C with 100% relative humidity to promote cell adhesion. The test samples were applied to the cells in successive concentrations after 24 hours. They were first dissolved in DMSO, and a sample solution was diluted with serum-free medium to twice the desired final maximum test concentration. To give a total of five sample concentrations, an additional four serial dilutions were made. Next, various sample dilutions were added in aliquots of 100 µL to the relevant wells that already had 100 µL of the medium, resulting in the necessary final sample concentrations. The plates were then exposed to 100% relative humidity for an additional 48 hours after the addition of the sample. For all concentrations, triplicate samples were maintained, and the medium containing no samples was used as the control.

3-[4, 5-dimethylthiazol-2-yl] 2, 5-diphenyltetrazolium bromide (MTT) assay was used for the evaluation of anticancer activity. Succinate dehydrogenase, a mitochondrial enzyme found in living cells, breaks the tetrazolium ring, turning the MTT into an insoluble purple formazan. As a result, the number of viable cells directly correlates with the amount of formazan generated. Each well received 15 µL of MTT (5 mg/mL) in phosphate-buffered saline (PBS) and was then incubated at 37°C for 4 hours of initial incubation. The generated formazan crystals were then dissolved in 100 µL of DMSO, and the MTT medium was turned off. A microplate reader

was then used to measure the absorbance at 570 nm (Monks *et al.*, 1991).

3. RESULTS AND DISCUSSION

3.1. UV-Visible and DRS Study

The UV-Vis absorption spectrum of the ZrO_2 NPs is shown in **Fig. 1.** The absorption maxima of Zr0.01, Zr0.02, and Zr0.03 were found to be 299, 302, and 307 nm, respectively. The sharp and prominent absorption peak agrees with the literature report of zirconia nanoparticles and may arise due to the transitions of electrons from the valence band to the conduction band. Similar results were observed for nanoparticles synthesised using many plant extracts. **Fig.** 2 displays the diffuse reflectance spectra of ZrO_2 NPs.

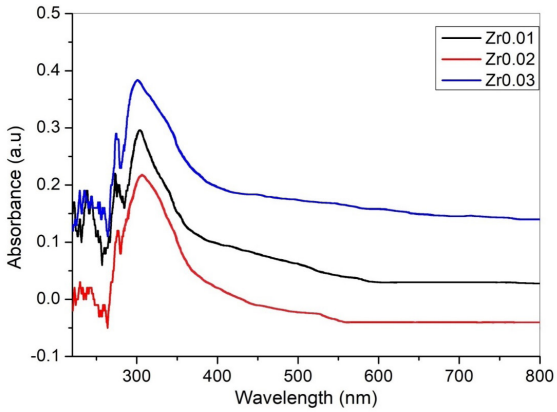

Figure 1. The absorption spectrum of ZrO_2 NPs (Zr0.01, Zr0.02 and Zr0.03).

The Tauc equation (1), which describes the link between absorbance and bandgap of the nanoparticles, was used to compute the bandgap energy of ZrO_2 NPs.

$$\alpha h\nu = K(h\nu - E_g)^n \quad (1)$$

Where α is the absorption coefficient, K is the constant, E_g is the bandgap energy of the samples, and n is equal to ½, 2, and 3/2 for direct and indirect allowed transitions, respectively. The graph is drawn as $(\alpha h\nu)^{1/2}$ versus energy ($h\nu$) due to the indirect bandgap energy of ZrO_2 NPs. These values closely match the bandgap values of zirconia nanoparticles that have been reported. Studying the bandgap energy of the samples reveals the minimum energy necessary for the excitation of an electron from a valence band to a conduction band (Suriyaraj *et al.*, 2019). The absorption phenomena were studied using the DRS, and the spectrum shown in **Fig.** 2 reveals that the maximum absorption occurred in the UV region and decreased with increasing wavelength. In **Fig.** 2, the curves show that the bandgap energies of Zr0.01, Zr0.02, and Zr0.03 correspond to 2.84, 3.18, and 3.20 eV, respectively. These values are in good agreement with the bandgap of nanoparticles synthesised in the literature reports (Haq *et al.*, 2018; Sirajul *et al.*, 2021).

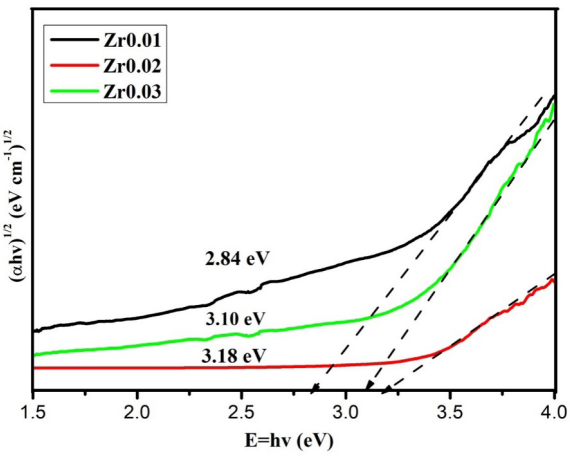

Figure 2. Bandgap energies of ZrO_2 NPs (Zr0.01, Zr0.02 and Zr0.03) from their absorption spectrum.

3.2. FTIR analysis

Functional groups were identified using the FTIR spectrum. The infrared spectra of Zr0.01, Zr0.02, and Zr0.03 are shown in **Fig.** 3, revealing the strong and weak absorption bands between 3300 and 3400 cm^{-1}. The water molecules on the samples in the FTIR spectrum exhibit a broad band at 3418 cm^{-1}, which is ascribed to their –OH stretching vibrations. The stretching vibrations of –OH and the bending vibrations of (H–O–H) and (O–H–O) found in samples are also responsible for the narrow band seen at 1627 cm^{-1}. Zr-O stretching modes are thought to be responsible for the weak band between 1149 and 1011 cm^{-1}. It is known that Zr–O–Zr vibrations have a distinct peak at 621 and 467 cm^{-1}. The presence of a peak at 530 cm^{-1} indicates the presence of Zr–OH vibrations. Possibly, phytochemicals present in the extract were found to be responsible for the development of hydroxide, which is transformed into oxide during the calcination at 500ºC by the loss of a water molecule (Adamczyk 2022).

 https://doi.org/10.37819/nanofab.10.2073

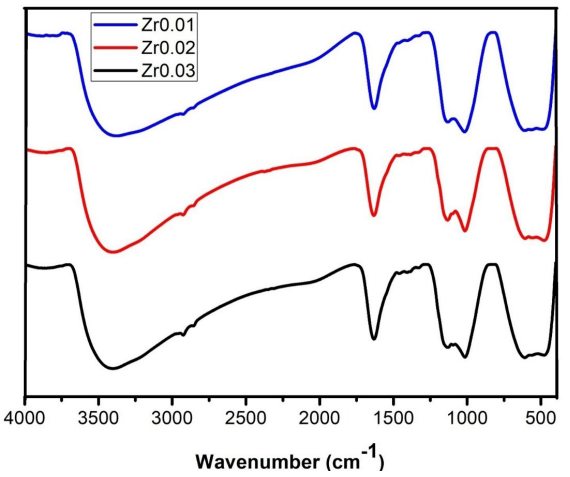

Figure 3. FTIR spectra of ZrO_2 NPs from the concentrations of Zr0.01, Zr0.02 and Zr0.03.

3.3. Structural Analysis

The crystalline nature and purity of the extract-stabilized zirconia nanoparticles were confirmed by the XRD pattern. **Fig. 4** shows the XRD pattern of ZrO_2 NPs synthesised using the extract at different concentrations. The diffraction peaks can be indicated at 2θ = 30.28, 34.85, 50.46, 60.07, and 74.24°, which were acknowledged for the diffractions of the (101), (110), (200), (211), and (202) crystalline planes of cubic phase ZrO_2 (JCPDS card no. 49-1642) (He *et al*., 2015). The cubic zirconia phase line is located at 2θ = 30.28° with a crystal size of 4 nm. There is no significant difference in the XRD patterns of Zr0.01, Zr0.02, and Zr0.3. The absence of additional peaks reveals the purity of the nanoparticles.

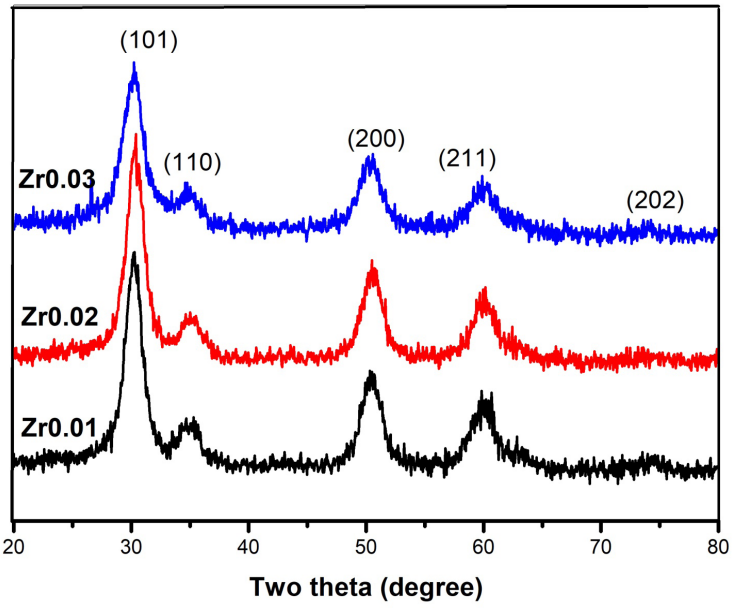

Figure 4. XRD spectra of ZrO_2 NPs from the concentrations of Zr0.01, Zr0.02 and Zr0.03.

It is noticeable that the plane (101) has the highest intensity, indicating that crystallites have grown uniformly along the plane (101). The smaller size of the particles is expressed by the broad diffraction peaks. The average crystallite size (D) of the particles was calculated using Scherer's formula (2).

$$D = 0.9\lambda/\beta\text{Cos}\,\theta \qquad (2)$$

Where λ = 1.5406Å (Cu-Kα), θ is the Bragg's diffraction angle, and β is the full width half maximum of the XRD peak (FWHM). The average crystallite sizes of the nanoparticles calculated using Scherrer's equation for Zr0.01, Zr0.02, and Zr0.03 were found to be ~4 nm.

3.4. Morphology and Elemental Analysis

Primarily, the formation of the particles was assessed by SEM morphology. **Fig. 5** (Zr0.01, Zr0.02 and Zr0.03 (i)) shows the SEM images of Zr0.01, Zr0.02, and Zr0.03, recorded at 2 µm. However, the shapes of nanoparticles are not clearly visible in SEM images due to exhibiting agglomerated particles. **Fig. 5(ii)** exhibits the percentage of zirconium and oxygen in Zr0.01, Zr0.02 and Zr0.03.

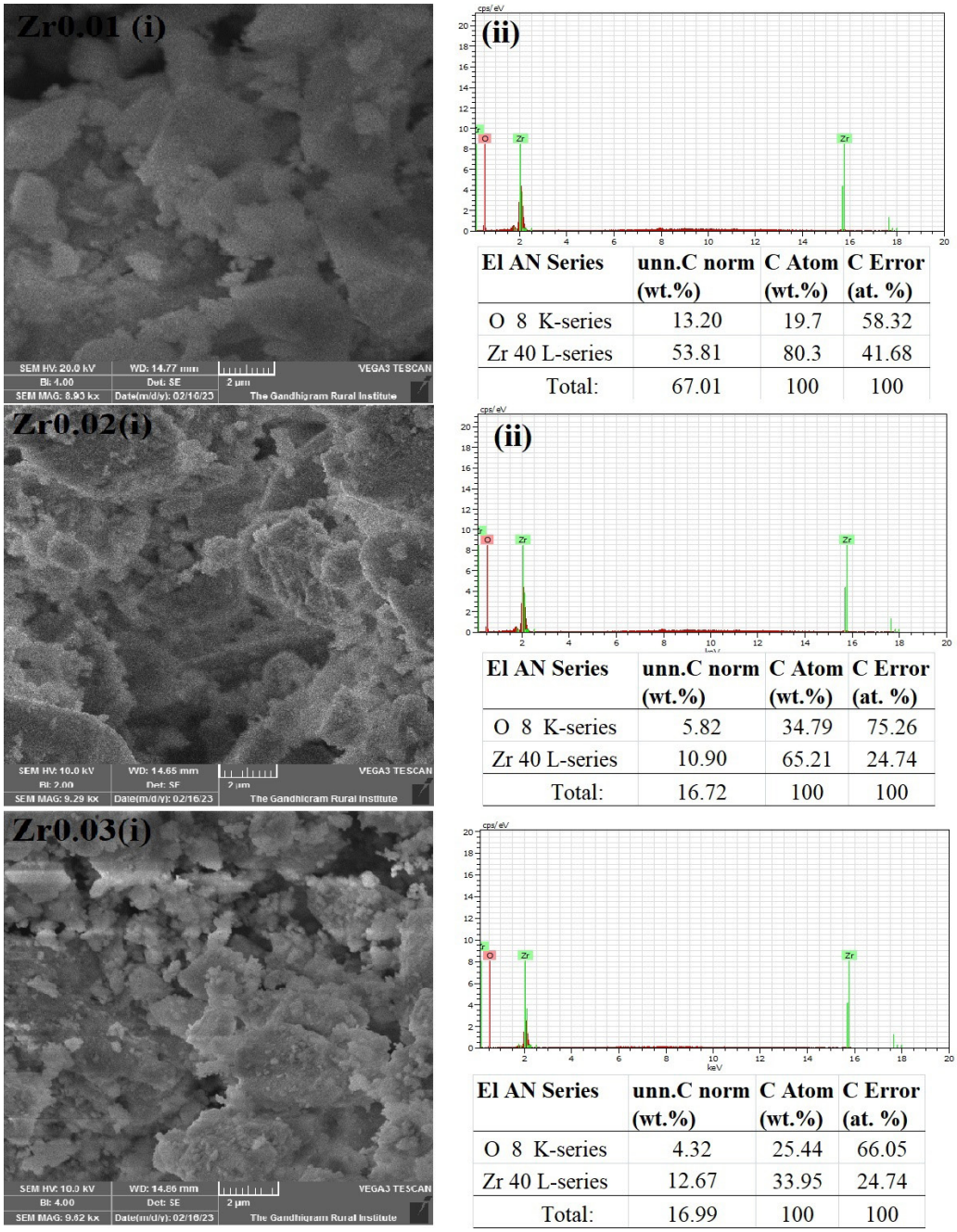

El AN Series	unn.C norm (wt.%)	C Atom (wt.%)	C Error (at. %)
O 8 K-series	13.20	19.7	58.32
Zr 40 L-series	53.81	80.3	41.68
Total:	67.01	100	100

El AN Series	unn.C norm (wt.%)	C Atom (wt.%)	C Error (at. %)
O 8 K-series	5.82	34.79	75.26
Zr 40 L-series	10.90	65.21	24.74
Total:	16.72	100	100

El AN Series	unn.C norm (wt.%)	C Atom (wt.%)	C Error (at. %)
O 8 K-series	4.32	25.44	66.05
Zr 40 L-series	12.67	33.95	24.74
Total:	16.99	100	100

Figure 5. SEM image of Zr0.01, Zr0.02 and Zr0.03 in around 8.5 (1000x) to 9.5 (1000x) with a 2 mm scale and the corresponding metal composition weight percentage of EDAX spectra.

The morphological study of the nanoparticles synthesised via the green method was analyzed through TEM images. As shown in **Fig. 6(i)** (Zr0.01, Zr0.02 and Zr0.03), the particles are exhibited and distributed uniformly. The TEM images reveal that the nanoparticles are well connected to their grain boundaries through their edges. The synthesised nanoparticles were perfectly crystallised, which is identified by the lattice in **Fig. 6**, noticed in the images. It is clear that the lattice fringes are evenly spaced along the length of the fringe. At different magnifications, the morphology of ZrO_2 NPs synthesised from 0.01, 0.02, and 0.03 M of precursor solution is found to be similar, including shape and

 https://doi.org/10.37819/nanofab.10.2073

distribution. As shown in **Fig. 6(ii)**, the selected area electron diffraction (SAED) exhibits bright spots all along the diffraction ring formed by the cubic structure of ZrO_2 NPs, confirming that the particles are smaller, highly crystallised, and perfectly connected through the grain boundaries.

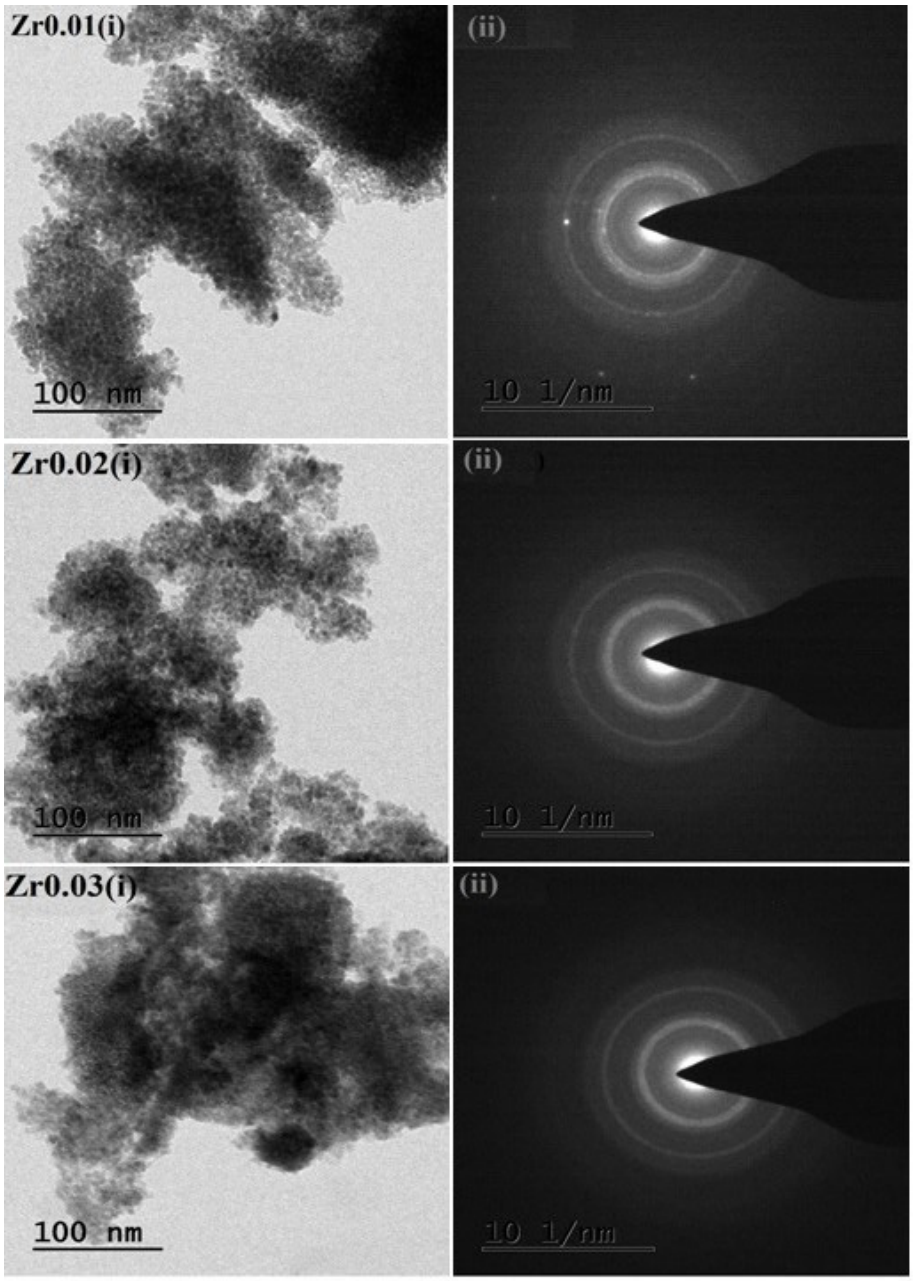

Figure 6. The morphology of TEM images of ZrO_2 NPs with compositions of Zr0.01, Zr0.02 and Zr0.03 at a 100 nm magnification scale (ii), the corresponding SAED pattern.

3.5. Antibacterial Activity

Green synthesised ZrO_2 NPs were tested for their antibacterial activity against gram-positive bacteria, namely, *L.acidophilus*, *S. albus*, and *S. mutans*. The nanoparticles Zr0.01, Zr0.02, and Zr0.03 showed 26, 28, and 32 mm zones of inhibition against *L. acidophilus*, *S. albus*, and *S.mutans* at the concentration of 25 µg/ml. The zone of ZrO_2 against these three bacteria is presented in **Table 2**.

Table 2. Zone of inhibition of ZrO_2 NPs at different concentrations.

		Zone of Inhibition (mm)			
Samples	**Bacteria**	**25 μg**	**50 μg**	**75 μg**	**Amoxicillin 10 μg**
Zr0.1	*Lactobacillus acidophilus*	8	8	32	34
	Staphylococcus albus	8	8	32	34
	Streptococcus mutans	8	8	30	34
Zr0.02	*Lactobacillus acidophilus*	8	12	26	32
	Staphylococcus albus	8	14	28	32
	Streptococcus mutans	8	16	28	32
Zr0.03	*Lactobacillus acidophilus*	8	8	28	34
	Staphylococcus albus	8	8	26	32
	Streptococcus mutans	8	8	32	34

The experiment was conducted in triplicate ($n = 3$)

The comparison zone of inhibition measured for ZrO_2 NPs is presented in **Fig. 7**. The ZrO_2 NPs exhibit a significant growth inhibitory effect against all these bacteria due to the smaller size and large surface area of the nanoparticles. Zr0.01, Zr0.02 and Zr0.03 showed effective bioactivity against selected bacterial pathogens, and the zones of inhibition were dose dependent as per three concentrations, i.e., 25, 50 and 75 μg/mL. However, the zone of inhibition of ZrO_2 NPs was less effective when compared with the amoxicillin standard. The difference in the zone of inhibition may be due to the following reasons: ZrO_2 NPs produce active species, which inhibit the accumulation of *L. acidophilus*, *S. albus*, and *S.mutans* on the surface of bacterial cells. It is understood that ZrO_2 NPs are able to effectively control the growth of these bacteria. It was reported that the size and shape of ZrO_2 NPs play a major role in killing bacteria and cancer cells. Smaller particles can have a larger zone of inhibition against bacteria and cancer cells. Many researchers have tested the antibacterial activity of ZrO_2 NPs. However, no zone of inhibition has been reported against some bacteria, such as *B. subtilis*, *S. mutans*, *S. aureus*, *E.coli*, *P. aeruginosa*, and *K. oxytoca* (Ayanwale *et al.*, 2020). and *S.aureus*. However, a 15 mm and 19 mm zone of inhibition against *Escherichia coli* has been reported (Jangra *et al.*, 2012; Ayanwale *et al.*, 2020).

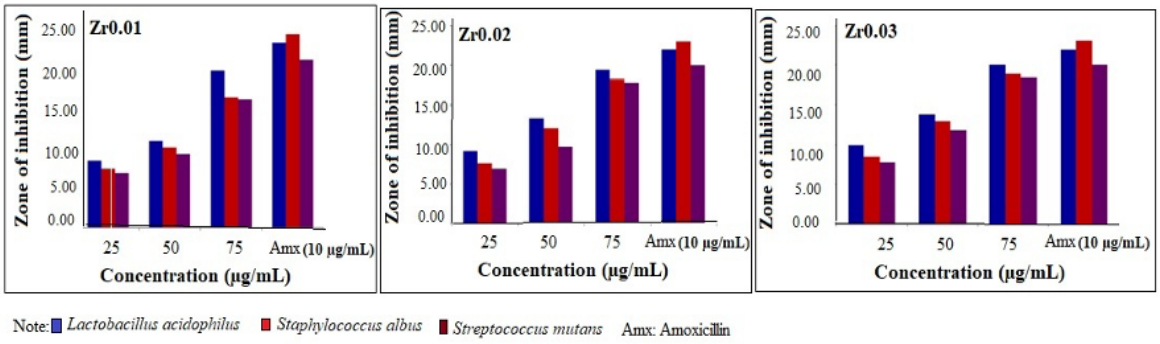

Figure 7. Antibacterial activity of ZrO_2 NPs against bacterial pathogens; (i) Zr. 0.01, (ii) Zr. 0.02, (iii) Zr. 0.03 concentrations.

3.6. Anticancer Activity

The anticancer activity of zirconia was tested on human lung cancer cell lines (A549). A dose-dependent cell viability test was carried out. The cell viability and IC_{50} values suggest that Zirconia is more toxic to A549 cell lines and has the potential for the development of anticancer drugs. The cell viability of A549 cells was tested by varying the concentrations of nanoparticles using by MTT assay. Cell viability was tested from 6.50 to 100 μg per mL. The growth inhibition was mentioned in percentage. The IC_{50} values of Zirconia were obtained from the graph drawn between the nanoparticles and the cell viability curve. As the concentration of nanoparticles increases, the toxicity decreases. As noticed in the im-

 https://doi.org/10.37819/nanofab.10.2073

ages, the morphology of A549 cells is increasingly tainted from normally stretched oblate to shatter, and this morphology inconsistency was actually noticed more after 24 hours. The percentage of cell viability is decreased with increasing concentrations of nanoparticles, as shown in **Fig. 8**.

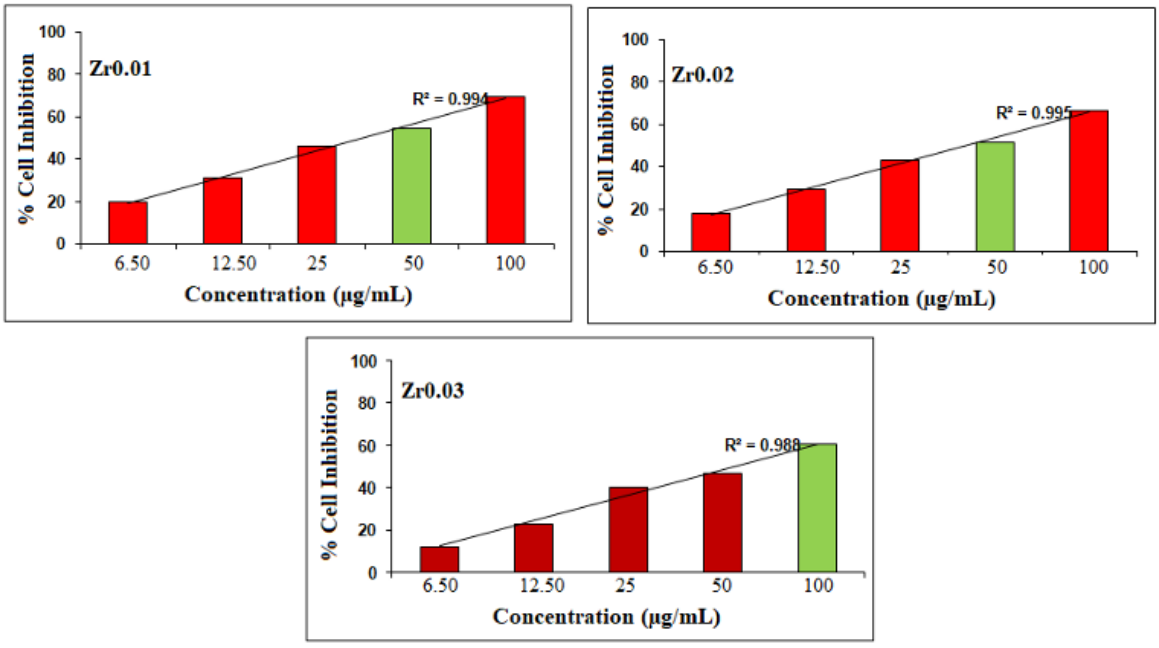

Figure 8. Lung cancer cells (A549) viability study of different concentrations of ZrO_2NPs.

The results indicate that the cell lines died due to a loss of membrane integrity. The IC_{50} values of Zr0.01, Zr0.02 and Zr0.03 were found to be 32.63, 42.39 and 68.60 µg/mL, respectively. The investigation of cell viability in response to various concentrations of nanoparticles is done using the MTT assay (Preetha *et al*., 2025). The figure depicts the cell viability of A549 cancer cells treated with ZrO_2 NPs at multiple doses. The higher concentration of ZrO_2 NPs at 100 µg/mL was shown to have the highest viability percentage. The dose-dependent cellular response profile is clearly shown in the images of ZrO_2 NPs treated with A549 cell lines (**Fig. 9**).

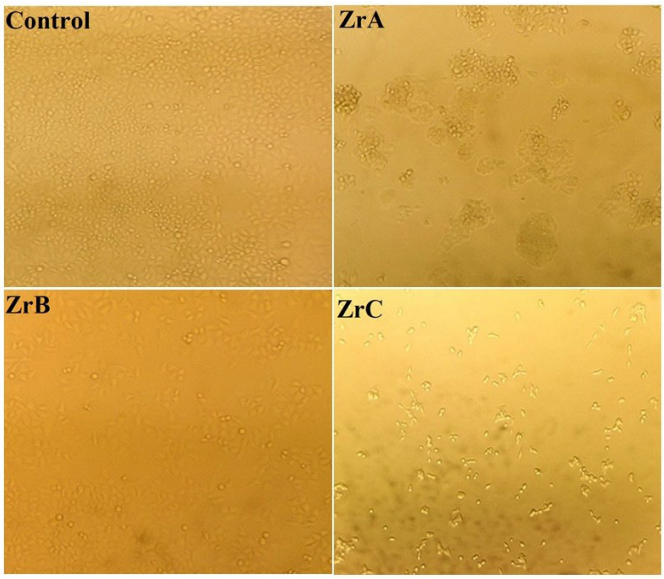

Figure 9. Optical microscopy images of A549 cells treated with ZrO_2 NPs (100 µg/mL): Control refer the image of normal A549 cells; Zr0.01, Zr0.02 and Zr0.03 represent the images of A549 cells treated with ZrO_2NPs at 100 µg/mL.

It was found that the anticancer activity might be seen in the lower concentration, indicating the phytochemical concentration is high, which had capped the nanoparticles. The microscopic study revealed that nanorods disrupt the cancerous cell membrane and kill A549 cancer cells, whereas untreated cells (control) tend to appear intact, as shown in **Fig. 9** (control). The IC_{50} values of Zr0.01 (32.63 µg/mL), Zr0.02 (42.39 µg/mL) and Zr0.03 (68.60 µg/mL) of *T. catappa* leaf extract stabilised ZrO Zr0.01 NPs. However, Zr0.01 exhibits efficient IC_{50} values, which suggest that the toxicity of nanoparticles depends on cell lines, stabilising agents, size and shape properties of the nanoparticles, considered as better compared with the literature reports. Tan *et al*., (2022) synthesised ZrO_2 nanoparticles with an average size of 20–60 nm using fruit peels of *Punica granatum* (Pomegranate). Analysis of the results revealed by Shah Reza *et al*., (2024) showed that the spherical nanoparticles with an average size 50 nm exhibited significant cytotoxic effects against human breast cancer cells. Similarly, Goyal *et al*., (2021) synthesised ZrO_2 nanoparticles with an average size of 40.59 nm using *Helianthus annuus* seed extract and revealed their effect against *S. aureus* and *E. coli*, *P. aeruginosa*, *K. pneumoniae*. The average sizes of ZrO_2 nanoparticles reported by other researchers are found to be in the range between 20–60 nm. However, very small and spherical nanoparticles with an average size of 4 nm obtained in this research are found to be better. Moreover, *Terminalia catappa* stabilized ZrO_2 showed an effective zone of inhibition against oral bacteria such as *L. acidophilus*, *S. albus*, and *S. mutans*. However, effect of concentration of Zr0.01, Zr0.02, and Zr0.03 on various cancer cell lines and bacteria will be considered as a future work and continued to understand the efficiency of ZrO_2 nanoparticles.

4. CONCLUSION

The smallest size ZrO_2 nanoparticles were successfully synthesized using aqueous fallen leaf extract of *T. catappa*. The XRD pattern and TEM morphology confirm that the green-synthesized zirconia nanoparticles are cubic and spherical, with an average size of 4 nm. The interaction of phytochemicals in *T. catappa* extract with zirconyl oxychloride solution led to the formation of zirconia nanoparticles. Oral bacteria, *Lactobacillus acidophilus*, *Staphylococcus albus*, and *Streptococcus mutans* exhibited 26, 28, and 32 mm zones of inhibition at the concentration of 25 µg/ml. Among the three nanoparticles, Zr0.01 showed the lowest IC_{50} value of 32.63 µg/mL against A549 cell lines. In conclusion, *T. catappa* leaf extract is an effective reducing agent for the synthesis of zirconia nanoparticles. The synthesised nanoparticles can be used for the development of antibacterial and anticancer agents.

Acknowledgement

Authors' contribution: Conceptualization, Methodology, and Supervision, RS; Investigation and Validation, PS; Validation and data curation, NT, PS; writing–original draft preparation and writing–review and editing, PB and RS; All authors have read and agreed to the published version of the manuscript.

Conflict of interest: The authors declare there is no conflict of interest in this research work.

Availability of data and materials: All data displayed in this publication are available from the corresponding author upon request.

References

Adamczyk, A. (2022). The Study of the Influence of ZrO_2 Precursor Type and the Temperature of Annealing on the Crystallization of the Tetragonal Polymorph of ZrO_2 in Zirconia-Silica Gels. *Gels.* 8, 724. https://doi.org/10.3390/gels8110724

Aishwarya, D., Vidya Shetty, K, & Saidutta, M.B. (2017). Highly stable silver nanoparticles synthesized using *Terminalia catappa* leaves as antibacterial agent and colorimetric mercury sensor. *Materials Letters*, 207, 66–71. https://doi.org/10.1016/j.matlet.2017.07.024

Altammar, K.A. (2023). A review on nanoparticles: characteristics, synthesis, applications, and challenges. *Frontier in Microbiology*, 14, 1155622. https://doi.org/10.3389/fmicb.2023.1155622

Annu, A., Sivasankari, C., & Ayyar Manikandan, A. (2022). Green synthesis and characterization studies of biogenic zirconium oxide (ZrO_2) nanoparticles for adsorptive removal of methylene blue dye. *Journal of Molecular Structure*, 1247, 131275. https://doi.org/10.1016/j.molstruc.2021.131275

Ayanwale, A.P., Ruíz-Baltazar, A., de J, Espinoza-Cristóbal, L., & Reyes-López, S.Y. (2020).

Bactericidal Activity Study of ZrO_2-Ag_2O Nanoparticles. *Dose-Response*, 18. https://doi.org/10.1177/1559325820941374

Banjara, R.A., Kumar,S., Aneshwari, R.K., Satnami, M.L., & Sinha, S.K. (2024). A comparative analysis of chemical vs green synthesis of nanoparticles and their various applications, Environmental Nanotechnology. *Monitoring & Management*, 22, 100988. https://doi.org/10.1016/j.enmm.2024.100988

Balaprasad, A. (2010). Biosynthesis of Gold Nanoparticles (Green-gold) using Leaf Extract of *Terminalia Catappa*. *E-Journal of Chemistry*, 7, 1334–1339. https://doi.org/10.1155/2010/745120

Chowdhury, M.A., Hossain, N., Golam Mostofa, M., Riyad Mia, M., Tushar, M., Masud Rana, M., & Helal Hossain, M. (2023). Green synthesis and characterization of zirconium nanoparticles for dental implant applications. *Heliyon*, 9, e12711. https://doi.org/10.1016/j.heliyon.2022.e12711

Castellin, A., Riello, P., & Carso, A (2021). Mesoporous zirconia nanoparticles as drug delivery systems: Drug loading, stability and release. *Journal of Drug Delivery Science and Technology*, 61,102189. https://doi.org/10.1016/j.jddst.2020.102189

De Jesus, R.A., De Assis, G.C., De Oliveira, R.J., Costa, J.R.S., P. Da Silva, C.M.P., Iqbal, H.M.N., & Ferreira, L.F.R. (2024). Metal/metal oxide nanoparticles: A revolution in the biosynthesis and medical applications. *Nano-Structures & Nano-Objects*, 37, 101071. https://doi.org/10.1016/j.nanoso.2023.101071

Dos Santos, O.V., Lorenzo, N.D., & da Silva Lannes, S.C. (2016). Chemical, morphological, and thermogravimetric of *Terminalia catappa* Linn. *Food Science and Technology*, 36, 151–158. https://doi.org/10.1590/1678-457X.0090

Goyal, P., Bhardwaj, A., Mehta, B.K., & Mehta, D. (2021). Research article green synthesis of zirconium oxide nanoparticles (ZrO_2NPs) using *Helianthus annuus* seed and their antimicrobial effects, *Journal of the Indian Chemical Society*, 98, 100089. https://doi.org/10.1016/j.jics.2021.100089

Haq, S., Rehman, W., Waseem, M., Meynen, V., Awan, S.U., Saeed, S., & Iqbal. N. (2018). Fabrication of pure and moxifloxacin functionalized silver oxide nanoparticles for photocatalytic and antimicrobial activity. *Journal of Photochemistry and Photobiology B Biology*, 186, 116–124. https://doi.org/10.1016/j.jphotobiol.2018.07.011

He, G., Wu, Y., Zhang, Y., Zhu, Y., Liu, Y., Li, N., …. & Mao, C. (2015). Addition of Zn to the ternary Mg–Ca–Sr alloys significantly improves their antibacterial properties. *Journal of Materials Chemistry B*, 3, 6676–6689. https://doi.org/10.1039/C5TB01319D

Ho, D.H., Doan, D.T., Nguyen, T. N., Ba, T. D., Do, Q. V., Pham, G. D., & Bui, K. A. (2022). Chemical Constituents from the leaves of *Terminalia catappa L.* (Combretaceae), *Vietnam Journal of Science and Technology*, 60, 625–630. https://doi.org/10.15625/2525-2518/15972

Jangra, S.L., Stalin, K., Dilbaghi, N., Kumar, S., Tawale, J., Singh, S.P., Pasricha, R. (2012). Antimicrobial Activity of Zirconia (ZrO_2) Nanoparticles and Zirconium Complexes. *Journal of Nanoscience and Nanotechnology*, 12, 7105–12. https://doi.org/10.1166/jnn.2012.6574

Kazi, S., Sandip Nirwan, S., Kunde, S., Jadhav, S., Rai, M., Kamble, D., Sayyed, S., & Chavan, P. (2022). Green Synthesis, Characterization and Bio-evaluation of Zirconium Nanoparticles Using the Dried Biomass of *Sphagneticola trilobata* Plant Leaf. *BioNanoScience*, 12, 731–740. https://doi.org/10.1007/s12668-022-01006-9

Lipsa, R., Mamata, D., & Jasaswini, T. (2023). *Terminalia catappa* leaf extract mediated ecofriendly synthesis of cerium oxide nanoparticles, Materials Today: Proceedings, https://doi.org/10.1016/j.matpr.2023.12.035

Monks, A., Scudiero, D., Skehan, P., Shoemaker, R., Paull, K., Vistica, D., … & Boyd, M. (1991). Feasibility of high flux anticancer drug screen using a diverse panel of cultured human tumour cell lines. *Journal of the National Cancer Institute*, 83, 757–766. https://doi.org/10.1093/jnci/83.11.757

Momoh, J. O., Kumar, S., Olaleye, O. N., Adekunle, O. M., & Aiyelero, T. S. (2024). Green synthesis of Characterized Bio-functionalized ZnO Nanoparticles from *Terminalia catappa* (Almond) Methanol Leaf Extract and their Potential Antioxidant and Antibacterial Properties. *Tropical Journal of Natural Product Research (TJNPR)*, 8, 9296-9309. https://doi.org/10.26538/tjnpr/v8i11.45

Muthulakshmi, L., Suganya, K., Murugan, M., Annaraj, J., Duraipandiyan, V., Al Farraj, D.A., … & Arockiaraj, J. (2022). Antibiofilm efficacy of novel biogenic silver nanoparticles from

Terminalia catappa against food-borne Listeria monocytogenes ATCC 15,313 and mechanisms investigation in-vivo and in-vitro. *Journal of King Saud University - Science*, 34, 102083. https://doi.org/10.1016/j.jksus.2022.102083

Muthulakshmi, N., Kathirvel, A., Senthil, M., & Subramanian, R., (2023). Green synthesis of zirconia nanoparticles and their characterization, anticancer activity and corrosion inhibition properties. *Journal of the Indian Chemical Society*, 100, 101076. https://doi.org/10.1016/j.jics.2023.101076

Nisha, K., Shweta, S., Meenakshi, V., Shelja, S., Ajay, S., Harvinder S.S., & Vishal, M. (2022). Zirconia-based nanomaterials: recent developments in synthesis and applications. *Nanoscale Advances*, 4, 4210–4236. https://doi.org/10.1039/D2NA00367H

Preetha, S., Anilkumar, P., & Nisha Jenifar, A. (2025). Comparative investigation of structural properties and biological applications of chemical and biogenic synthesis of zirconium dioxide (ZrO_2) nanoparticles using *Passiflora edulis*. *Journal of Photochemistry and Photobiology B: Biology*, 263, 113089. https://doi.org/10.1016/j.jphotobiol.2024.113089

Razieh, A., Zahra, S., & Majid, H. (2022). Synthesis of ZnO Nanoparticles with Antibacterial Properties Using *Terminalia catappa* Leaf Extract. *Chemical Engineering Technology*, 45, 658–666. https://doi.org/10.1002/ceat.202100430

Sarala, E., Vinuth, M., Madhukara Naik, Y.V., & Rami, R. (2022). Green synthesis of nickel ferrite nanoparticles using *Terminalia catappa*: Structural, magnetic and anticancer studies against MCF-7 cell lines. *Journal of Hazardous Materials Advances*, 8, 100150, https://doi.org/10.1016/j.hazadv.2022.100150

Shah Reza, M.A., Golnaraghi-Ghomi, A., Rasouli, A., Rasouli Asl, F., Dadashpour, M., Sokhansanj, A., … & Movahhed, T.K. (2024). Green Synthesis, Characterization and Biological activity of Optimized *Alfalfa*-Mediated Zirconium Nanoparticles, *ChemistrySelect*, 9, e202400914. https://doi.org/10.1002/slct.202400914

Suresh Ramanan, S, A., Arunachalam, Rinku, S., & Ankit, V. (2025). Tropical almond (*Terminalia catappa*): A holistic review. *Heliyon*, 11, e41115. https://doi.org/10.1016/j.heliyon.2024.e41115

Suriyaraj, S.P., Ramadoss, G., Chandraraj, K., & Selvakumar, R. (2019). One pot facile green synthesis of crystalline bio-ZrO_2 nanoparticles using *Acinetobacter sp*. KCSI1 under room temperature. *Materials Science & Engineering C*, 105, 110021. https://doi.org/10.1016/j.msec.2019.110021

Sirajul, H., Humma, A., Manel Ben, A., Mohammed, A., Bander, A., …. & Amor, H. (2021). Green Synthesis and Characterization of a ZnO-ZrO_2 Heterojunction for Environmental and Biological Applications. *Crystals*, 11, 1502. https://doi.org/10.3390/cryst11121502

Tan, P. C., Geetha, R. V., Mathiyazhagan, N., Arunachalam, C., Sulaiman, A. A., Baskaran, S., …. & Surachai, P. (2022). Green synthesis of Zirconium nanoparticles using *Punica granatum* (pomegranate) peel extract and their antimicrobial and antioxidant potency. *Environmental Research*, 209, 112771. https://doi.org/10.1016/j.envres.2022.112771

Thi Hoai, P.Nguyen., Thi Phuong, N., Thi Anh, T. N., Tien, D.N., Woong, C., Duc, N., & Duong, L. (2024). *Terminalia catappa* leaf extract as a bio-reducing agent to synthesize Cu_2O nanoparticles for methylene blue photodegradation. *Discovery Applied Sciences*, 6, 309. https://doi.org/10.1007/s42452-024-05990-3

Veerabhadraswamy, B.N., Pradeep, H. K., Swaroop, K., Manoj, K.M., Dhanush Nadigar, M.V., Akash PateL, M.P., & Bhagya, N.P. (2024). Green synthesis and characterization of zirconium oxide with antimicrobial activities. *iop conference series: materials science and engineering*, 1300, 012036. https://doi.org/10.1088/1757-899x/1300/1/012036

Wang, Q., Li, J., Liu, H., Zhao, X., Huang, H., Dong, W.C., Gui, R., … & Nie, X (2021) Zirconia Nanoparticles Induce HeLa Cell Death Through Mitochondrial Apoptosis and Autophagy Pathways Mediated by ROS. *Frontiers in Chemistry*, 9, 5227082. https://doi.org/10.3389/fchem.2021.522708

Weerasekara, W., Rathnayaka, R., & Saranandha, K.H. (2015). Preparation of ready-to-serve beverage from tropical almond (*Terminalia cattappa*) fruit pulp. *Tropical Agricultural Research and Extension*, 15, 105–107. https://doi.org/10.4038/tare.v15i4.5260

Wangui, C. M., Walyambillah, W., Madivoli, E.S., & Joyline, G. (2024). Phytochemical characterization, antimicrobial and antioxidant activities of *Terminalia catappa* methanol and aqueous extracts, Global web icon. *BMC Complementary Medicine and Therapies*, 24, 137. https://doi.org/10.1186/s12906-024-04449-7